

Affordance-Aware Interactive Decision-Making and Execution for Ambiguous Instructions

Hengxuan Xu^{1,2,*}, Fengbo Lan^{1,2,*}, Zhixin Zhao¹, Shengjie Wang³, Mengqiao Liu¹,
Jieqian Sun¹, Yu Cheng^{4,†}, Tao Zhang^{1,†}

¹Department of Automation, Tsinghua University, Beijing, China

²Shanghai Artificial Intelligence Laboratory, Shanghai, China

³Institute for Interdisciplinary Information Sciences, Tsinghua University, Beijing, China

⁴Computer Science and Engineering Department, Chinese University of Hong Kong, Hong Kong, China

Abstract

Enabling robots to explore and act in unfamiliar environments under ambiguous human instructions by interactively identifying task-relevant objects (e.g., identifying cups or beverages for “I’m thirsty”) remains challenging for existing vision-language model (VLM)-based methods. This challenge stems from inefficient reasoning and the lack of environmental interaction, which hinder real-time task planning and execution. To address this, We propose Affordance-Aware Interactive Decision-Making and Execution for Ambiguous Instructions (AIDE), a dual-stream framework that integrates interactive exploration with vision-language reasoning, where Multi-Stage Inference (MSI) serves as the decision-making stream and Accelerated Decision-Making (ADM) as the execution stream, enabling zero-shot affordance analysis and interpretation of ambiguous instructions. Extensive experiments in simulation and real-world environments show that AIDE achieves the task planning success rate of over 80% and more than 95% accuracy in closed-loop continuous execution at 10 Hz, outperforming existing VLM-based methods in diverse open-world scenarios. Video demonstrations of real-world experiments and more information can be found on the [supplementary website](#).

1 Introduction

Ambiguous task understanding and object affordance reasoning remain significant challenges for intelligent robotic systems [Cheng *et al.*, 2024], particularly in complex, dynamic, and open environments. Humans can interpret ambiguous instructions by evaluating environmental context and adapting their actions accordingly. In daily human-human and human-machine interactions, commands often omit explicit details. For example, when someone says “I am thirsty,” as illustrated in Figure 1, people may choose to fetch a cup or a bottle of water, or use a bowl if a bottle is unavailable. Similarly, in unfamiliar scenes, successful task execution requires repeated interaction and exploration of both the environment and hu-

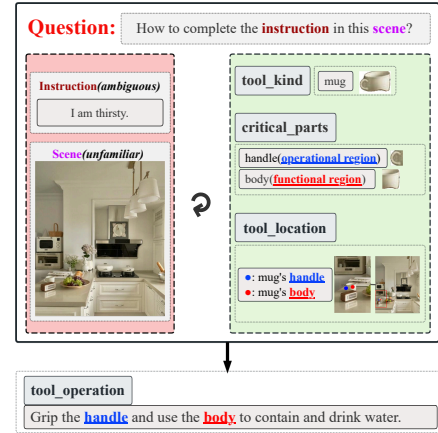


Figure 1: Method objective. Given ambiguous instruction and unfamiliar scene as the input task, the ultimate objective of the AIDE method is to find the required tool and locate its operational and functional regions within the scene, enabling the robot to operate the tool accurately and complete the task.

mans, along with understanding the affordances and functions of available tools to support effective decision-making.

Recent advances in large language models (LLMs) and vision-language models (VLMs) have shown strong abilities in conceptual understanding, common-sense reasoning, and semantic knowledge representation [Chowdhery *et al.*, 2023; Devlin *et al.*, 2018; Li *et al.*, 2023; Ramesh *et al.*, 2022]. In particular, these models encode extensive world knowledge [Parisi *et al.*, 2022; Jiang *et al.*, 2020; Gurnee and Tegmark, 2023]. Trained on large-scale Internet data, VLMs can recognize objects and infer their basic functions, such as identifying a cup as a tool for drinking water. However, their ability to reason about object affordances remains limited. For example, given the task “I want to crack walnuts,” humans can flexibly choose alternative tools, such as a heavy book or another object with sufficient weight and rigidity, when a hammer is unavailable, whereas current VLMs cannot. Moreover, using VLMs for ambiguous task understanding and planning in open-ended environments often leads to hallucinations and uncertainty due to the lack of environmental interaction. Their online inference is also expensive and

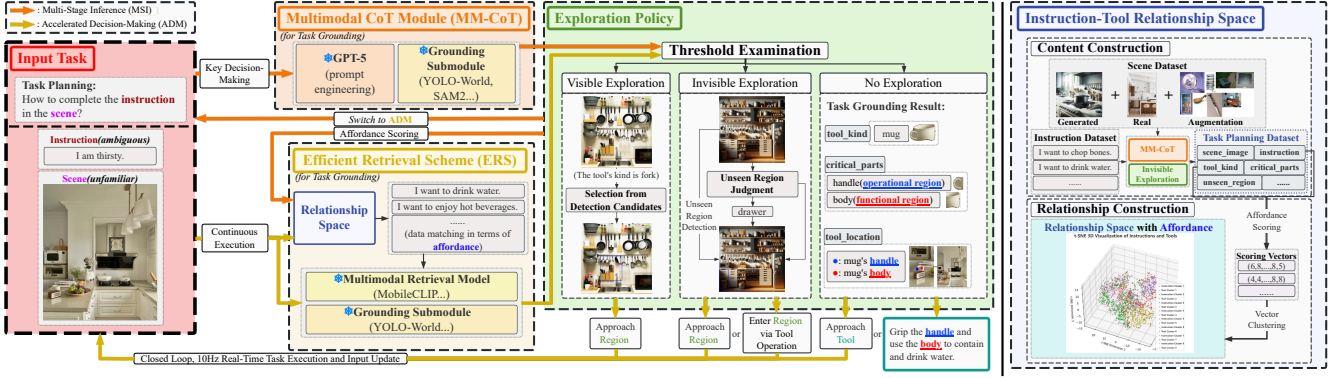


Figure 2: Framework of the AIDE. Given the input task, the Multi-Stage Inference (MSI) stream uses Multimodal CoT Module (MM-CoT) and Exploration Policy to generate keyframe-based task planning result. By scoring the input instruction based on affordance, this result is projected into the Instruction-Tool Relationship Space, enabling a sufficient cross-modal understanding of the input instruction and robustness to hallucinations arising from GPT-5 reasoning. Building on this projection, the Accelerated Decision-Making (ADM) stream employs Efficient Retrieval Scheme (ERS) and Exploration Policy for real-time, closed-loop task execution over continuous frames.

slow, limiting the applicability of VLMs to real-world task planning and execution.

To address these challenges, we propose AIDE, a novel vision-language task planning framework featuring a cross-coupled dual-stream mechanism for reasoning and decision-making (Figure 2). AIDE provides an efficient closed-loop planning approach based on interactive exploration. Unlike conventional methods that rely solely on Vision-Language Models (VLMs), AIDE significantly enhances a robot’s task understanding and planning under ambiguous human instructions by actively interacting with the environment and, when needed, with humans to acquire, update, and integrate missing information in real time.

AIDE Components and Performance 1) **Task Planning Framework.** AIDE employs a reasoning-decision dual-stream architecture, where Multi-Stage Inference (MSI) acts as the decision-making stream and Accelerated Decision-Making (ADM) serves as the execution stream. The framework includes four key parts: • **Multimodal Chain-of-Thought (CoT) Module:** Enables zero-shot understanding and planning for ambiguous tasks. • **Instruction-Tool Relationship Space:** Establishes task-tool associations to guide analysis of critical object affordances. • **Efficient Retrieval Scheme:** Supports faster and more consistent decision-making. • **Interaction Exploration Policy:** Promotes active exploration and interaction, enhancing generalization to unseen environments and tasks. 2) **Experimental Performance.** AIDE achieves a task-level decision frequency of 10 Hz and over 80% accuracy across 400 test samples, surpassing state-of-the-art task planning methods. These results highlight AIDE’s effectiveness as a general-purpose robotic system capable of handling ambiguous human instructions.

2 Related Work

Visual Language Models and Large Language Models. The remarkable progress achieved by LLMs [OpenAI, 2025; Chowdhery *et al.*, 2023; Toussaint *et al.*, 2018] has sparked increased interest in VLMs [Gan *et al.*, 2022; OpenAI, 2023;

Xu *et al.*, 2018]. The general approach of VLMs is to use cross-modal connectors to maintain alignment between the features of the pre-trained visual encoder and the input space of LLMs, while generating single-step planning results in an end-to-end manner. Research on Chain of Thought (CoT) has further led to the integration of step-wise reasoning and execution capabilities within VLMs and LLMs. Our study focuses on leveraging CoT [Cheng *et al.*, 2024] to guide robots in task planning within scenarios, thereby addressing tasks that involve uncertainty.

Pre-Trained Foundation Models For Robotics. The application of large pretrained foundation models to advance robot technology can be categorized into three types: Pre-trained Visual Models, Pretrained Language Models, Pre-trained Visual Language Models. Many studies have investigated the application of pretrained foundation models like visual language models (VLMs) in robotic technology [Du *et al.*, 2023; Gao *et al.*, 2023; Huang *et al.*, 2023; Sacerdoti, 1975]. Notably, RT-2 [Brohan *et al.*, 2023] demonstrated the integration of VLMs in low-level robot control. In contrast, our research primarily focuses on high-level planning for robots. While Palm-E [Driess *et al.*, 2023], MOKA [Liu *et al.*, 2024], and our method share similarities, they typically require extensive training with large-scale visual-language datasets [Chen *et al.*, 2022; Lynch *et al.*, 2023]. VILA [Hu *et al.*, 2023] and Copa [Liang *et al.*, 2023] concentrate more on tasks involving clearly specified commands, complete information, and relatively single-scenario tasks. Our work, however, is more concerned with addressing challenges related to ambiguous task understanding, planning, and interactive exploration, especially in multi-object and multi-scale open environments.

Task and Motion Planning [Garrett *et al.*, 2021] is a key framework for addressing long-distance planning tasks, integrating low-level continuous motion planning [LaValle, 2006] with high-level discrete task planning [Fikes and Nilsson, 1971; Ren *et al.*, 2023]. While traditional research has primarily focused on symbolic planning [Nau *et al.*, 1999]

or optimization-based methods [Sutton and Barto, 2018; Toussaint, 2015], the advent of machine learning [Ichter *et al.*, 2020; Xie *et al.*, 2023] and LLMs [Chen *et al.*, 2023; Ding *et al.*, 2023] is reshaping this domain. The introduction of Visual Language Action (VLA) methods [Kim *et al.*, 2024; Wen *et al.*, 2025] has further shifted the focus toward end-to-end task execution. Our approach builds on visual language models (VLMs), incorporating the physical properties of objects to construct a sparse instruction scene corpus that contains rich information, such as instructions, scenarios, tool attributes, and tool images. This enables efficient task planning with an execution frequency that meets the requirements of closed-loop control.

3 Method

In this section, we introduce the AIDE framework (Figure 2), which alternates between two complementary streams, namely Multi-Stage Inference (MSI) for key decision-making and Accelerated Decision-Making (ADM) for continuous execution, to support accurate planning and real-time closed-loop execution for the input task comprising the ambiguous instruction and the unfamiliar scene, progressing towards the objective in Figure 1. The two streams are realized through four core parts: the Multimodal CoT Module (MM-CoT) for task grounding, the affordance-aware Instruction-Tool Relationship Space, the Efficient Retrieval Scheme (ERS), and the Interactive Exploration Policy. We next detail the MSI and ADM streams, followed by the four core parts.

3.1 Framework

Given the input task, AIDE dynamically alternates between two streams during task execution. The MSI stream is invoked once for key decision-making when the task is novel or ADM fails to identify any valid tool-related object in the updated scene (by applying a threshold based on the detection confidence produced and similarity matching), producing the task planning result stored for subsequent ADM retrieval. In all other cases, AIDE relies on the ADM stream for continuous execution.

Multi-Stage Inference Stream

For the MSI stream, the input task is first processed by the MM-CoT and the Exploration Policy to produce the task planning result, which is then projected into the Instruction-Tool Relationship Space for storage and indexing. This projection is implemented via DFS-based instruction retrieval in the ERS, which leverages the affordance vector of the input instruction computed under the affordance scoring formulation of the relationship space. Through this process, the MSI-generated result is located in the relationship space, and the candidate task planning results associated with the input task are retrieved; together, they support sufficient cross-modal understanding of the input instruction and robustness to hallucinations arising from GPT-5 reasoning for subsequent ADM retrieval and matching.

Accelerated Decision-Making Stream

The ADM stream enables closed-loop, real-time task execution by continuously performing task planning and updating

the scene through robot interaction. Given the input task, the ADM performs task planning through the ERS and the Exploration Policy, with the former process relying on retrieval from a pool comprising retrieved candidate and MSI-generated task planning results. Operating in a closed-loop manner with real-time input updates at 10 Hz, ADM leverages exploration results from task planning to determine the robot’s motion strategy as follows: (1) visible exploration: the robot approaches the exploration region. (2) invisible exploration: the robot approaches the region when distant or temporarily reformulates the instruction for planning on key regions to enable entry into the exploration region when nearby, before resuming the original instruction. (3) no exploration: the robot approaches the tool region when distant or directly manipulates the operational and functional regions to complete the task. By instructing the robot to execute the corresponding motion strategy, the input scene is continuously updated.

3.2 Multimodal CoT Module

The MM-CoT receives the input task and, through prompt-engineered multimodal CoT, jointly leverages GPT-5’s [OpenAI, 2025] multimodal reasoning capability and the grounding submodule’s localization ability to produce the task grounding result, including labels, images and locations for the required tool and its critical parts. Together, these outputs enable task planning that focuses on instruction completion within the scene.

Concretely, upon receiving the input task, GPT-5 first predicts the target tool label and its key attributes. This information is passed to the grounding submodule, where the object detection model YOLO-World [Cheng *et al.*, 2024] and the image segmentation model SAM2 [Ravi *et al.*, 2024] process the scene to identify the top- N candidate tools based on detection confidence. These candidates are returned to GPT-5, which integrates label and attribute cues to select the most appropriate instance and outputs its identifier. The identifier is then used by SAM2, in coordination with GPT-5, to segment the corresponding tool, distinguishing its operational and functional regions, thus completing the entire multimodal CoT task grounding process.

3.3 Instruction-Tool Relationship Space

The Instruction-Tool Relationship Space is built by generating instruction-indexed task planning results as content, and then by establishing many-to-many instruction-tool relationships among them as the primary goal, while also inducing instruction-instruction and tool-tool relationships with functional roles. Accordingly, this space is constructed through two key processes: content construction based on the MM-CoT and the Exploration Policy, and relationship construction derived from affordance analysis.

For the former process, diverse instructions and scenes are ensured to yield valid task planning results, which serve as the content. We first use GPT-5 to generate A instructions, which are then made ambiguous to adopt a natural, everyday tone and exclude explicit tool labels. And we construct three types of scene datasets: (1) scene images generated by DALL-E 3 [Betker *et al.*, 2023] (Generated Scene Dataset),

(2) real-world scene images containing instruction-relevant tools sourced from the Internet (Real Scene Dataset), and (3) data augmentation images combining required tools with distractors from ImageNet dataset [Deng *et al.*, 2009] (Augmentation Scene Dataset). Each instruction is paired with three scene images sampled from the three datasets. For each instruction-scene pair, the task grounding result indexed by the instruction is generated by the MM-CoT, and the label and image of the unseen region are produced by the invisible exploration stage of the Exploration Policy, which will be described later. These results undergo GPT-5-based format validation and manual screening to filter out erroneous or hallucinated ones, thereby ensuring that each ambiguous instruction indexes three valid task grounding results and unseen regions. Thus, the A ambiguous instructions, their corresponding three types of scene images, the valid task grounding results, and unseen regions form the Task Planning Dataset, namely the content of the relationship space.

For the latter process, we perform affordance scoring and clustering on each ambiguous instruction together with the tool image in its indexed task planning results. We first define affordance for tools as their ability, by virtue of their physical properties, to satisfy human instruction requirements through interaction, and for instructions as the ability that tools must have to complete them. Based on this, we use GPT-5 to perform affordance scoring over X dimensions (specified via the GPT-5 prompt design) for each instruction and a randomly sampled tool image from its indexed three task planning results in the Task Planning Dataset, yielding X -dimensional affordance vectors. These vectors exhibit largely overlapping distributions for instructions and tools, both of which can be clustered separately into a groups via k-means (Figure 3), with most vectors concentrated near cluster centers and a small fraction scattered as noise, potentially due to hallucinations of GPT-5. These observations reveal that the affordance vectors scored from instructions and located near cluster centers capture category-level affordances shared by both instructions and their required tools, naturally inducing many-to-many instruction-tool, instruction-instruction, and tool-tool relationships across different task planning results. Based on this, we select the T instructions as indexes, whose affordance vectors, together with those of their corresponding tool images, lie within a Euclidean distance D of and are closest to their respective cluster centers. We further use k-means to organize them into a clusters with b subclusters each, to facilitate efficient indexing and retrieval. Together, the task planning results indexed by the T instructions and the induced relationships form the whole relationship space.

3.4 Efficient Retrieval Scheme

The ERS takes the input task and employs multimodal retrieval models (e.g., MobileCLIP [Vasu *et al.*, 2024]) together with grounding models (e.g., YOLO-World). It performs efficient matching between the input and retrieved candidate task planning results obtained via affordance-based retrieval from the Instruction-Tool Relationship Space. Based on a similarity-based threshold, the scheme outputs either a complete task grounding result or retrieved candidate task planning results.

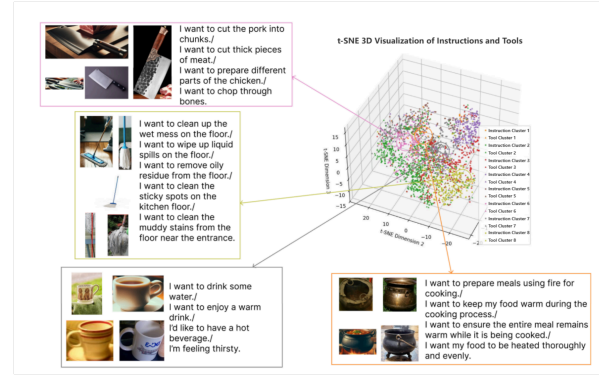


Figure 3: Affordance vector distributions for instructions and tools after t-SNE projection into the three-dimensional space. The image shows that taking cutting/cleaning/drinking/heating-related tasks as representative examples, the affordance vector distributions for instructions and tools largely overlap.

Specifically, given the input instruction, the scheme performs an affordance-based depth-first search (DFS) over clusters in the relationship space until selecting an instruction whose affordance vector lies within a Euclidean distance c of the input. It then retrieves instructions from the same sub-cluster whose tool affordance vectors are within a Euclidean distance d , with each retrieved instruction indexing its associated task planning result. Based on these retrieved candidate task planning results indexed from the relationship space, the ERS uses YOLO-World to detect the top- N candidate tools in the input scene, ranked by detection confidence. MobileCLIP is then applied to compute multimodal similarities between these candidates and the tool images in the indexed results, and the candidate with the highest similarity is retrieved as the required tool. And this highest similarity, constrained to be less than 1, is denoted as S_{\max} . If S_{\max} exceeds m , the detection and similarity-matching procedure is repeated within the retrieved tool region to identify the operational and functional regions, thus generating the complete task grounding result analogous to that of the MM-CoT. Otherwise, the ERS outputs the retrieved candidate task planning results for the Exploration Policy.

3.5 Exploration Policy

Given the input task, when S_{\max} exceeds m , exploration is skipped, and the task grounding result from MM-CoT or ERS is directly output. Otherwise, in complex scenes where the required tool is distant, occluded, or barely visible, the Exploration Policy localizes a rectangular region likely containing the tool to support subsequent approach and execution. In such cases, two interactive exploration strategies are employed: visible exploration and invisible exploration.

Visible Exploration: Assuming that the required tool is visible but blurred due to its distance from the robot, if the required tool is unlikely to be among the top N candidate tools based on the detection confidence in the YOLO-World model, it is more likely to be found in areas with high confidence ranked from $(N + 1)$ to N' , due to the underlying principle

that objects with higher detection confidence in YOLO-World are more likely to be closer to the true detection label. Based on this, the interactive visible exploration strategy accumulates and compares detection weights in square regions with a radius of PX pixels, centered on each candidate tool ranked $(N + 1)$ to $2N$ in YOLO-World. The weight for each square region is accumulated based on objects ranked from $(N + 1)$ to N' that intersect or are contained within it, with the weight for each valid object calculated as $N' - rank_{conf}$, where $rank_{conf}$ denotes the rank of detection confidence. The minimal bounding rectangle including both the region with the highest accumulated weight and all intersecting objects is finally chosen, thus completing the visible exploration.

Invisible Exploration: When the required tool is not directly visible (e.g., occluded and undetected by YOLO-World), the invisible exploration outputs the unseen region where the required tool may exist but is unseen. When the unseen region list from the externally provided retrieved candidate task planning results is available, we use MobileCLIP to select the unseen region label by matching the input with labels in the provided list; otherwise, the label is inferred by GPT-5 from the input. Based on the selected label, YOLO-World retrieves the top N candidate unseen region images according to detection confidence. The final exploration region is determined by matching the candidate images with the unseen region images in the provided list when it is available, or by using GPT-5 to select from the candidate images.

4 Experiment

This section details the simulation and real-world experiment design, along with analysis of the results and key characteristics of the AIDE. Through comparisons with state-of-the-art baselines, ablation studies, and error analysis, we validate the design and effectiveness of AIDE, as well as the contributions of its core innovations, including affordance analysis and the exploration policy, which together enable AIDE to achieve higher task completion accuracy and efficiency.

4.1 Experimental Setup

a) Baseline: We compare AIDE with eight baselines: Molmo-7B-D-0924 [Deitke *et al.*, 2024], Qwen3-VL-30B-A3B-Instruct [Team, 2025], GPT-5, Magma-8B [Yang *et al.*, 2025], Robopoint-v1-vicuna-v1.5-13b [Yuan *et al.*, 2024], SayCan, MOKA, and IntroPlan (direct) [Liang *et al.*, 2024]. Among them, the first three are advanced MLLMs with varying model sizes; the next two are VLMs tailored for downstream robot manipulation; and the last three are methods specifically developed for robotic task planning.

b) Simulation Experiment Setting: This part presents the simulation setting and test set construction. We empirically set the parameters as $A=1,500$, $D=25$, $T=1,368$, $X=19$, $a=8$, $b=3$, $c=10$, $d=15$, $m=0.85$, $N=5$, $N'=40$, and $PX=250$ for AIDE task planning and execution. In simulation, AIDE is implemented following the MSI-ADM process described in the framework, taking the task as input and producing task planning results via ADM. And the AIDE operates on a subsampled Instruction-Tool Relationship Space. This space contains 432 instructions selected from the entire

set of $T=1,368$ instructions. The subsample is constructed based on task planning results indexed by 32 cluster-node instructions and 400 randomly sampled instructions, together with their associated relationships. As shown in Table 4, the average naturalness scores assigned by different LLMs to all instructions involved in AIDE, IntroPlan, and MOKA indicate that the instructions used in AIDE achieve average scores above 6 across multiple criteria and are substantially higher than those of the other two baselines. This demonstrates that the instructions in AIDE are ambiguous yet expressed in a more natural tone, consistent with the description in Section 3.3. Based on this observation, we construct two test sets, termed G-Dataset and R-Dataset, by randomly sampling 100 instructions from the remaining 936 instructions in the entire Instruction-Tool Relationship Space and pairing them with 200 images drawn respectively from the Generated Scene Dataset and the Real Scene Dataset, yielding 200 instruction-scene pairs for each test set. As the Augmentation Scene Dataset lacks realistic context, it is excluded to enable a faithful evaluation of AIDE’s interactive exploration. The resulting test sets cover diverse scenarios, including cases where tools are either clearly identifiable, ambiguous, unrecognizable, or absent, thereby supporting a rigorous assessment of AIDE’s closed-loop interactive exploration under realistic indoor conditions.

c) Real-World Experiment Setting: In real-world experiments, we use a 6-DOF wheeled robotic arm with the AIDE method deployed on its host. Given six ambiguous instructions, labeled Instructions 1-6: “I am thirsty”, “I want to clean the dust”, “I want to crack walnuts”, “I want something cold to drink”, “I want to close up delivery boxes tightly”, and “I want to support my waist while sitting”, the robot is tested in a cluttered indoor environment for its ability to navigate toward the region where the required tool is located in real-time and grasp it appropriately.

4.2 Simulation Result and Discussion

Comparison Experiments: We compare the zero-shot task planning performance of AIDE against eight baselines on the G-Dataset and R-Dataset. As shown in Table 1, AIDE achieves task planning success rates above 80%, with 83% on the G-Dataset and 88% on the R-Dataset, exceeding all baselines by over 30%. It is also noteworthy that AIDE achieves tool selection success rates of approximately 95% (94.5% on the G-Dataset and 95.0% on the R-Dataset), outperforming all baselines, which validates the effectiveness and robustness against hallucination of the MM-CoT design in the MSI stream of the AIDE, as well as the efficiency and well-chosen hyperparameters of the affordance-analysis-based ERS in the ADM stream. And we further conduct ablation studies on the hyperparameter settings for ERS’s affordance retrieval (see the supplementary material for details), thereby providing additional evidence supporting the above findings. Together, the designs of MSI and ADM ensure efficient and reliable tool selection. For the remaining metrics, namely operational and functional region selection success rates, AIDE also consistently ranks first among all baselines. All above results verify the effectiveness of the AIDE framework in task planning for ambiguous instructions in unfamiliar scenes. In addition,

Method	Functionality			G-Dataset						R-Dataset					
	CL	AA	RT	TSR	OSR	FSR	WSR	ASR	FPS	TSR	OSR	FSR	WSR	ASR	FPS
Molmo				10.5	6.5	1.0	0.5	0.0	0.05	15.5	9.5	4.0	1.5	0.0	0.05
Qwen3-VL				42.0	23.5	13.5	12.0	8.0	0.04	70.0	31.0	34.5	21.0	5.0	0.04
GPT-5				50.5	34.5	37.5	29.5	<u>12.0</u>	0.03	78.0	37.0	45.5	33.5	<u>10.0</u>	0.04
Magma		✓		1.5	0.0	0.5	0.0	0.0	<u>1.03</u>	1.0	0.5	0.0	0.0	0.0	<u>0.94</u>
Robopoint	✓			64.0	38.0	34.0	21.5	4.0	0.14	77.5	41.5	38.5	36.5	0.0	0.19
SayCan	✓	✓		42.5	-	-	-	-	0.04	59.0	-	-	-	-	0.03
MOKA	✓			81.5	<u>57.5</u>	<u>53.5</u>	<u>49.0</u>	-	0.03	<u>88.0</u>	<u>68.5</u>	<u>59.0</u>	<u>54.0</u>	-	0.03
IntroPlan				<u>82.0</u>	-	-	-	-	0.04	87.5	-	-	-	-	0.04
AIDE	✓	✓	✓	94.5	88.0	89.0	83.0	64.0	9.70	95.0	92.0	91.0	88.0	65.0	9.50

Table 1: Zero-shot performance comparison on G-Dataset and R-Dataset. “TSR”, “OSR”, “FSR” and “WSR” denotes tool, operational region, functional region selection, and whole task planning success rate, respectively. “ASR” denotes the task planning success rate in tool-absent scenes. “FPS” denotes the average execution rate per test sample for each method. “CL”, “AA”, and “RT” represent closed-loop, affordance analysis, and real-time execution functionalities, respectively. **Bold** indicates the best performance for each metric, while underlined indicates the second-best performance. “-” means not supported. All success rates are evaluated via majority vote from three random evaluators, and are reported in percentage (%) except FPS.

Method	G-Dataset						R-Dataset					
	TSR	OSR	FSR	WSR	ASR	FPS	TSR	OSR	FSR	WSR	ASR	FPS
AIDE (w/o ADM)	90.5	89.0	84.5	80.5	68.0	0.03	96.0	91.5	90.0	87.0	70.0	0.03
AIDE (w/o MSI)	<u>92.5</u>	79.5	<u>84.5</u>	74.0	52.0	9.70	93.0	82.0	86.0	79.0	50.0	9.50
AIDE (Full)	94.5	<u>88.0</u>	89.0	83.0	64.0	9.70	<u>95.0</u>	92.0	91.0	88.0	<u>65.0</u>	9.50

Table 2: Ablation study on different components of AIDE. AIDE (w/o ADM) and AIDE (w/o MSI) represent AIDE variants that rely solely on the designed MSI and ADM, respectively, while AIDE (Full) represents the complete framework comprising both MSI and ADM.

Stream	G-Dataset		R-Dataset	
	EDR	ERR	EDR	ERR
ADM	63.5	-	57.1	-
MSI	-	41.0	-	42.3

Table 3: Error Detection and Recovery Performance of AIDE. EDR (Error Detection Rate) measures the proportion of failed test cases in Table 1 for which ADM correctly identifies errors by detecting the absence of valid tool-related objects in the scene. Upon detection, ADM switches to MSI. ERR (Error Recovery Rate) measures the proportion of failed test cases in the same table that MSI successfully recovers through human interaction, including tool reselection and further exploration, without invoking ADM. Both metrics are reported as percentages (%).

we isolate instruction-scene pairs from the G-Dataset and R-Dataset in which the target tools are not detectable, and evaluate the exploration capability of AIDE and baselines on these cases, measured by the task planning success rate in tool-absent scenes. The results show that all baselines capable of exploration achieve success rates below 15% on this metric, whereas AIDE exceeds 60% on both test sets (64.0% on the G-Dataset and 65.0% on the R-Dataset), outperforming other baselines by over 45%. These results validate AIDE’s supe-

rior exploration capability and the effectiveness of interactive exploration policy. For the FPS metric, only AIDE achieves nearly 10 Hz, while all baselines except Magma operate below 0.2 Hz. Although Magma attains close to 1 Hz due to its lightweight, it exhibits the lowest success rates on both test sets designed for complex embodied planning. These results validate that AIDE simultaneously achieves high accuracy and high efficiency in task planning.

Ablation Experiments: Table 6 reports ablation results on MSI and ADM in AIDE. Ablation studies show that incorporating the ADM stream enables AIDE to achieve efficient affordance-based retrieval, matching or surpassing MSI-only performance on most metrics, with task planning success rate gains of 2.5% and 1% on the G-Dataset and R-Dataset, respectively, and a 320× FPS increase to nearly 10 Hz. And incorporating the MSI stream allows AIDE to leverage GPT-5-based scene understanding, resulting in 2%-15% improvements across success rate metrics. Together, these results highlight both the distinct roles of MSI and ADM and their complementary synergy in improving the accuracy and efficiency of task planning and execution. In addition, we further conduct ablation studies on other critical components of AIDE (see the supplementary material for details).

Functionality Analysis Columns 2-4 of Table 1 present the functionality comparison between AIDE and baselines.

Method	Qwen3-Next-80B	Llama3-70B	GPT-5
AIDE	6.43	6.67	7.45
IntroPlan	3.22	4.12	5.99
MOKA	1.47	2.67	3.27

Table 4: Instruction Naturalness Analysis. Average naturalness scores (1-10) of instructions from different methods, as evaluated by different LLMs; higher score indicates higher naturalness.

No.	Instruction (abbr.)	Valid Frames	ESR (%)
1	Thirsty	937	96.1
2	Clean dust	656	96.8
3	Crack walnuts	1180	97.9
4	Drink cold	850	97.2
5	Close up boxes	924	97.4
6	Support waist	333	99.7

Table 5: Zero-shot performance on Instructions in real-world experiments. Instruction (abbr.) means abbreviated instructions. “Valid Frames” means the number of frames captured by the robot-mounted camera from task initiation to the moment before the successful tool grasp. “ESR” denotes continuous task execution success rate calculated on valid frames.

Among them, SayCan [Ahn *et al.*, 2022] and AIDE support closed-loop planning, while affordance analysis is incorporated into Robopoint, SayCan, MOKA and AIDE. Magma and AIDE enable real-time planning. In particular, AIDE uniquely achieves real-time (10 Hz) closed-loop planning by combining affordance analysis with the interactive exploration policy, highlighting its advantage over other baselines.

4.3 Real-World Experiments

In real-world experiments, the robot successfully performs real-time task planning and execution under Instructions 1-6 through interactive exploration, namely grasping the cup, brush, hammer, and pillow for Instructions 1-3 and 6, respectively, and locating the Coke in the fridge and the tape in the drawer for Instructions 4-5. And for Instructions 4-5, the grasping is omitted due to its redundancy with other tasks’ final grasping steps. The results above demonstrating the real-time capability and robustness of the interactive exploration-based closed-loop AIDE framework in complex scenarios. As shown in Figure 4, AIDE performs visible exploration to localize distant but observable targets (bottom left). When sufficiently close, ERS is used to identify the target tool’s operational and functional regions (top left and bottom middle) or the tool itself (top right and bottom right). In contrast, invisible exploration is triggered when the target is unlikely to appear in visible regions (top middle), enabling AIDE to realize in real-world experiments the functionalities demonstrated in simulation.

Table 5 reports the AIDE’s continuous task execution success rate across six tasks, with over 95% on valid frames in all cases. This high performance, observed under continuous execution from the robot’s egocentric view, highlights the framework’s closed-loop robustness in real-world settings,

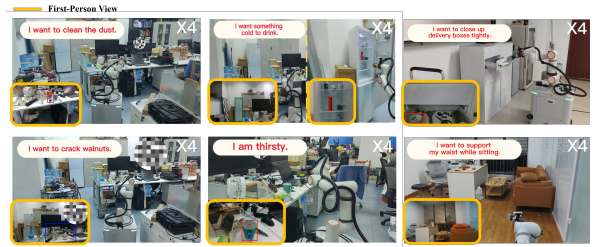


Figure 4: Examples of real-world experiment results. Top left and bottom middle: Identified handle (blue dot) and body (red dot) regions of the target tool. Bottom left: Visible exploration region (blue box). Top middle: Invisible exploration region (green box). Top right and bottom right: tool region (red box).

thereby strengthening the credibility of the task planning success rate in simulation experiments.

4.4 Error Analysis

During task planning and execution, AIDE may encounter errors (Table 1), classified as planning-level or perception-level errors. Planning-level errors arise from incorrect task understanding, potentially causing planning or execution failures. When these occur in ADM, the system checks for valid tool-related objects and switches to MSI if none are found. Failures in MSI are often due to occasional hallucinations from GPT-5, despite the MM-CoT design, and can be mitigated through human interaction for tool re-identification and further exploration. We separately extracted test cases from Table 6 where ADM and MSI failed, and evaluated ADM’s error detection rate and MSI’s error recovery rate. As shown in Table 3, ADM’s detection rate exceeds 50% and MSI’s recovery rate exceeds 40% across both test sets, demonstrating the effectiveness of these mechanisms. Perception-level errors occur when task understanding is correct but visual degradation from robot motion causes small offsets in area-tool positioning. These manifest as sporadic single-frame deviations amid predominantly correct execution frames. As reported in Table 5, such errors account for only 0.3-3.9% of valid frames and do not impact overall task completion.

5 Conclusions

We propose AIDE, a novel framework that enables robots to interactively explore and execute tasks under ambiguous instructions in complex indoor environments. AIDE first employs MSI to generate task planning results, which are projected into the affordance-based Instruction-Tool Relationship Space comprising over 1000 task samples. It then leverages ADM for multimodal retrieval and interactive exploration to support real-time closed-loop execution. Simulation and real-world experiments demonstrate that affordance analysis and interactive exploration significantly improve task planning and execution, and that AIDE outperforms state-of-the-art baselines in both accuracy and efficiency, highlighting its strong potential for real-world deployment. Overall, AIDE represents a substantial advancement in robot task planning, facilitating future research on efficiently handling ambiguous instructions in complex and dynamic environments.

References

[Ahn *et al.*, 2022] Michael Ahn, Anthony Brohan, Noah Brown, Yevgen Chebotar, Omar Cortes, Byron David, Chelsea Finn, Chuyuan Fu, Keerthana Gopalakrishnan, Karol Hausman, et al. Do as i can, not as i say: Grounding language in robotic affordances. *arXiv preprint arXiv:2204.01691*, 2022.

[Betker *et al.*, 2023] James Betker, Gabriel Goh, Li Jing, Tim Brooks, Jianfeng Wang, Linjie Li, Long Ouyang, Juntang Zhuang, Joyce Lee, Yufei Guo, et al. Improving image generation with better captions. *Computer Science*. <https://cdn.openai.com/papers/dall-e-3.pdf>, 2(3):8, 2023.

[Brohan *et al.*, 2023] Anthony Brohan, Noah Brown, Justice Carabajal, Yevgen Chebotar, Xi Chen, Krzysztof Choromanski, Tianli Ding, Danny Driess, Avinava Dubey, Chelsea Finn, et al. Rt-2: Vision-language-action models transfer web knowledge to robotic control. *arXiv preprint arXiv:2307.15818*, 2023.

[Chen *et al.*, 2022] Xi Chen, Xiao Wang, Soravit Changpinyo, AJ Piergiovanni, Piotr Padlewski, Daniel Salz, Sebastian Goodman, Adam Grycner, Basil Mustafa, Lucas Beyer, et al. Pali: A jointly-scaled multimodal language-image model. *arXiv preprint arXiv:2209.06794*, 2022.

[Chen *et al.*, 2023] Yongchao Chen, Jacob Arkin, Yang Zhang, Nicholas Roy, and Chuchu Fan. Autotamp: Auto-generative task and motion planning with llms as translators and checkers. *arXiv preprint arXiv:2306.05531*, 2023.

[Cheng *et al.*, 2024] T. Cheng, L. Song, Y. Ge, et al. Yoloworld: Real-time open-vocabulary object detection. In *Proceedings of the IEEE/CVF Conference on Computer Vision and Pattern Recognition*, pages 16901–16911, 2024.

[Chowdhery *et al.*, 2023] Adakraksha Chowdhery, Sharan Narang, Jacob Devlin, Maarten Bosma, Gavin Mishra, Adam Roberts, Paul Barham, Hyung Won Chung, Charles Sutton, Sebastian Gehrmann, et al. Palm: Scaling language modeling with pathways. *Journal of Machine Learning Research*, 24(240):1–113, 2023.

[Deitke *et al.*, 2024] Matt Deitke, Christopher Clark, Sangho Lee, Rohun Tripathi, Yue Yang, Jae Sung Park, Mohammadreza Salehi, Niklas Muennighoff, Kyle Lo, Luca Soldaini, Jiasen Lu, Taira Anderson, Erin Bransom, Kiana Ehsani, Huong Ngo, YenSung Chen, Ajay Patel, Mark Yatskar, Chris Callison-Burch, Andrew Head, Rose Hendrix, Favyen Bastani, Eli VanderBilt, Nathan Lambert, Yvonne Chou, Arnavi Chheda, Jenna Sparks, Sam Skjonsberg, Michael Schmitz, Aaron Sarnat, Byron Bischoff, Pete Walsh, Chris Newell, Piper Wolters, Tanmay Gupta, Kuo-Hao Zeng, Jon Borchardt, Dirk Groeneveld, Jen Dumas, Crystal Nam, Sophie Lebrecht, Caitlin Wittlif, Carissa Schoenick, Oscar Michel, Ranjay Krishna, Luca Weihs, Noah A. Smith, Hannaneh Hajishirzi, Ross Girshick, Ali Farhadi, and Aniruddha Kembhavi. Molmo and pixmo: Open weights and open data for state-of-the-art multimodal models. *arXiv preprint arXiv:2409.17146*, 2024.

[Deng *et al.*, 2009] Jia Deng, Wei Dong, Richard Socher, Li-Jia Li, Kai Li, and Li Fei-Fei. Imagenet: A large-scale hierarchical image database. In *2009 IEEE conference on computer vision and pattern recognition*, pages 248–255. Ieee, 2009.

[Devlin *et al.*, 2018] Jacob Devlin, Ming-Wei Chang, Kenton Lee, and Kristina Toutanova. Bert: Pre-training of deep bidirectional transformers for language understanding. *arXiv preprint arXiv:1810.04805*, 2018.

[Ding *et al.*, 2023] Yan Ding, Xiaohan Zhang, Chris Paxton, and Shiqi Zhang. Task and motion planning with large language models for object rearrangement. *arXiv preprint arXiv:2303.06427*, 2023.

[Driess *et al.*, 2023] Danny Driess, Fei Xia, Mehdi SM Sajjadi, Corey Lynch, Aakanksha Chowdhery, Brian Ichter, Ayzan Wahid, Jonathan Thompson, Quan Vuong, Tianyu Xu, et al. Palm-e: An embodied multimodal language model. *arXiv preprint arXiv:2303.03378*, 2023.

[Du *et al.*, 2023] Yuting Du, Ksenia Konyushkova, Misha Denil, Akhil Raju, Jessica Landon, Felix Hill, Nando de Freitas, and Serkan Cabi. Vision-language models as success detectors. *arXiv preprint arXiv:2303.07280*, 2023.

[Fikes and Nilsson, 1971] Richard E Fikes and Nils J Nilsson. Strips: A new approach to the application of theorem proving to problem solving. *Artificial intelligence*, 2(3-4):189–208, 1971.

[Gan *et al.*, 2022] Zhe Gan, Linjie Li, Chunyuan Li, Lijuan Wang, Zicheng Liu, Jianfeng Gao, et al. Vision-language pre-training: Basics, recent advances, and future trends. *Foundations and Trends® in Computer Graphics and Vision*, 14(3-4):163–352, 2022.

[Gao *et al.*, 2023] Jensen Gao, Bidipata Sarkar, Fei Xia, Ted Xiao, Jiajun Wu, Brian Ichter, Anirudha Majumdar, and Dorsa Sadigh. Physically grounded vision-language models for robotic manipulation. *arXiv preprint arXiv:2309.02561*, 2023.

[Garrett *et al.*, 2021] Caelan Reed Garrett, Rohan Chitnis, Rachel Holladay, Beomjoon Kim, Tom Silver, Leslie Pack Kaelbling, and Tomás Lozano-Pérez. Integrated task and motion planning. *Annual review of control, robotics, and autonomous systems*, 4:265–293, 2021.

[Gurnee and Tegmark, 2023] Wes Gurnee and Max Tegmark. Language models represent space and time. *arXiv preprint arXiv:2310.02207*, 2023.

[Hu *et al.*, 2023] Y. Hu, F. Lin, T. Zhang, et al. Look before you leap: Unveiling the power of gpt-4v in robotic vision-language planning. *arXiv preprint arXiv:2311.17842*, 2023.

[Huang *et al.*, 2023] Wenlong Huang, Chen Wang, Ruohan Zhang, Yunzhu Li, Jiajun Wu, and Li Fei-Fei. Voxposer: Composable 3d value maps for robotic manipulation with language models. *arXiv preprint arXiv:2307.05973*, 2023.

[Ichter *et al.*, 2020] Brian Ichter, Pierre Sermanet, and Corey Lynch. Broadly-exploring, local-policy trees for long-

horizon task planning. *arXiv preprint arXiv:2010.06491*, 2020.

[Jiang *et al.*, 2020] Zhengbiao Jiang, Frank F Xu, Jun Araki, and Graham Neubig. How can we know what language models know? *Transactions of the Association for Computational Linguistics*, 8:423–438, 2020.

[Kim *et al.*, 2024] M. J. Kim, K. Pertsch, S. Karamcheti, et al. Openvla: An open-source vision-language-action model. *arXiv preprint arXiv:2406.09246*, 2024.

[LaValle, 2006] Steven M LaValle. *Planning algorithms*. Cambridge university press, 2006.

[Li *et al.*, 2023] Junnan Li, Dongxu Li, Silvio Savarese, and Steven Hoi. Blip-2: Bootstrapping language-image pre-training with frozen image encoders and large language models. *arXiv preprint arXiv:2301.12597*, 2023.

[Liang *et al.*, 2023] Jacky Liang, Wenlong Huang, Fei Xia, Peng Xu, Karol Hausman, Brian Ichter, Pete Florence, and Andy Zeng. Code as policies: Language model programs for embodied control. In *2023 IEEE International Conference on Robotics and Automation (ICRA)*, pages 9493–9500. IEEE, 2023.

[Liang *et al.*, 2024] Kaiqu Liang, Zixu Zhang, and Jaime Fernández Fisac. Introspective planning: Aligning robots’ uncertainty with inherent task ambiguity. In *The Thirty-eighth Annual Conference on Neural Information Processing Systems*, 2024.

[Liu *et al.*, 2024] F. Liu, K. Fang, P. Abbeel, et al. Moka: Open-vocabulary robotic manipulation through mark-based visual prompting. In *First Workshop on Vision-Language Models for Navigation and Manipulation at ICRA 2024*, 2024.

[Lynch *et al.*, 2023] Corey Lynch, Ayzan Wahid, Jonathan Thompson, Tianli Ding, James Better, Robert Barruch, Travis Armstrong, and Pete Florence. Interactive language: Talking to robots in real time. *IEEE Robotics and Automation Letters*, 2023.

[Nau *et al.*, 1999] Dana Nau, Yael Cao, Amnon Lotem, and Hector Munoz-Avila. Shop: Simple hierarchical ordered planner. In *Proceedings of the 16th international joint conference on Artificial intelligence-Volume 2*, pages 968–973, 1999.

[OpenAI, 2023] OpenAI. Gpt-4 [vision] system card. Technical report, 2023.

[OpenAI, 2025] OpenAI. Gpt-5 system card. Technical report, 2025.

[Parisi *et al.*, 2022] Simone Parisi, Arvind Rajeswaran, Senthil Purushwalkam, and Abhinav Gupta. The unsurprising effectiveness of pre-trained vision models on control. In *International Conference on Machine Learning*, pages 17359–17371. PMLR, 2022.

[Ramesh *et al.*, 2022] Aitya Ramesh, Mikhail Pavlov, Gabriel Goh, Scott Gray, Chelsea Voss, Alec Radford, Mark Chen, and Ilya Sutskever. Zero-shot text-to-image generation. In *International Conference on Machine Learning*, pages 8821–8831. PMLR, 2022.

[Ravi *et al.*, 2024] N. Ravi, V. Gabeur, Y. T. Hu, et al. Sam 2: Segment anything in images and videos. *arXiv preprint arXiv:2408.00714*, 2024.

[Ren *et al.*, 2023] Allen Z Ren, Anushri Dixit, Alexandra Bodrova, Sumeet Singh, Stephen Tu, Noah Brown, Peng Xu, Leila Takayama, Fei Xia, Jaike Varley, et al. Robots that ask for help: Uncertainty alignment for large language model planners. *arXiv preprint arXiv:2307.09128*, 2023.

[Sacerdoti, 1975] Earl D Sacerdoti. *A structure for plans and behavior*. PhD thesis, Department of Computer Science, Stanford University, 1975.

[Sutton and Barto, 2018] Richard S Sutton and Andrew G Barto. *Reinforcement learning: An introduction*. MIT press, 2018.

[Team, 2025] Qwen Team. Qwen3 technical report, 2025.

[Toussaint *et al.*, 2018] Marc A Toussaint, Kelsey Rebecca Allen, Kevin A Smith, and Joshua B Tenenbaum. Differentiable physics and stable models for tool-use and manipulation planning. 2018.

[Toussaint, 2015] Marc Toussaint. Logic-geometric programming: An optimization-based approach to combined task and motion planning. In *IJCAI*, pages 1930–1936, 2015.

[Vasu *et al.*, 2024] Pavan Kumar Anasosalu Vasu, Hadi Pouransari, Fartash Faghri, Raviteja Vemulapalli, and Oncel Tuzel. Mobileclip: Fast image-text models through multi-modal reinforced training. In *Proceedings of the IEEE/CVF Conference on Computer Vision and Pattern Recognition (CVPR)*, June 2024.

[Wen *et al.*, 2025] J. Wen, Y. Zhu, J. Li, et al. Tinyvla: Towards fast, data-efficient vision-language-action models for robotic manipulation. *IEEE Robotics and Automation Letters*, 2025.

[Xie *et al.*, 2023] Yaqii Xie, Chen Yu, Tongyao Zhu, Jinbin Bai, Ze Gong, and Harold Soh. Translating natural language to planning goals with large-language models. *arXiv preprint arXiv:2302.05128*, 2023.

[Xu *et al.*, 2018] Danfei Xu, Suraj Nair, Yuke Zhu, Julian Gao, Animesh Garg, Li Fei-Fei, and Silvio Savarese. Neural task programming: Learning to generalize across hierarchical tasks. In *2018 IEEE International Conference on Robotics and Automation (ICRA)*, pages 3795–3802. IEEE, 2018.

[Yang *et al.*, 2025] Jianwei Yang, Reuben Tan, Qianhui Wu, Ruijie Zheng, Baolin Peng, Yongyuan Liang, Yu Gu, Mu Cai, Seonghyeon Ye, Joel Jang, Yuquan Deng, Lars Liden, and Jianfeng Gao. Magma: A foundation model for multimodal ai agents, 2025.

[Yuan *et al.*, 2024] Wentao Yuan, Jiafei Duan, Valts Blukis, Wilbert Pumacay, Ranjay Krishna, Adithyavairavan Murali, Arsalan Mousavian, and Dieter Fox. Robopoint: A vision-language model for spatial affordance prediction for robotics. *arXiv preprint arXiv:2406.10721*, 2024.

A Environment setting

This section introduces the more detailed hardware and software conditions of the experiments related to the paper. For the simulation experiment of AIDE, the hardware platform has an Intel 8360Y CPU and an RTX A6000 GPU. The deployment platform for the real-machine experiment is an Advantech Industrial control computer without a GPU. The robotic arm used is the FAIRINO FR - 3 robot with 6 DOF, the gripper is the Agibot omnipicker x1, and a RealSense D435 camera, as shown in Figure 5. The software environment mainly depends on CUDA 12.1, Python 3.10, and torch 2.3.1.

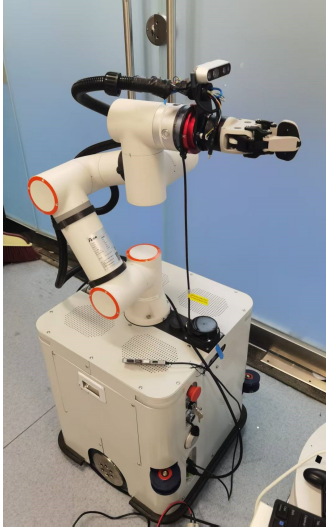


Figure 5: The robot used to conduct the real-world experiment has 2 wheels, a 6 DOF arm, a gripper, and a RealSense camera.

B Details of the Instruction-Tool Relationship Space

B.1 Scene dataset example

As described in the paper, to support content generation for the Instruction-Tool Relationship Space, we construct three types of scene datasets: the Generated Scene Dataset, the Real Scene Dataset, and the Augmentation Scene Dataset. Representative samples from these datasets are illustrated in Figure 6.

B.2 Space content example

As described in the paper, the constructed Task Planning Dataset serves as the content of the Instruction-Tool Relationship Space. As illustrated in Figure 7, each piece of data in this dataset consists of three main components: (1) the input instruction and scene image, where the former serves as the index; (2) the task grounding result generated by the MM-CoT, including tool label and image, annotated operational and functional regions; and (3) region label and image indicating potential tool locations when not directly visible, inferred via GPT-5 and YOLO-World.



Figure 6: Scene dataset samples. Three scene samples from three distinct datasets used to construct the Instruction-Tool Relationship Space: generated (left), real (middle), and augmentation (right).

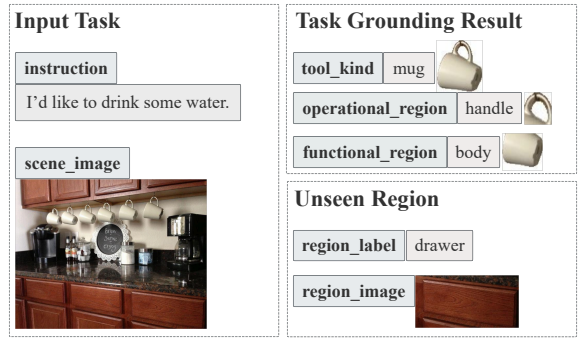


Figure 7: A data sample from the Task Planning Dataset consisting of three parts: the input task comprising the scene image and instruction; the valid task grounding result generated by the MM-CoT; and the label and image of the unseen region where the tool is not directly visible.

B.3 Filtering pipeline for task planning results

As mentioned in the paper, all data included in the content of the Instruction-Tool Relationship Space are subjected to a filtering pipeline to ensure the validity of the relationship space. The detailed procedure is as follows: Each data instance is first validated using GPT-5-based format checking and manual screening to identify erroneous or hallucinated results. Identified cases are addressed by replacing the corresponding scene image with a new one sampled from the same scene dataset and regenerating the task planning result. This process is performed iteratively, where the results from each round are used as input for validation and screening in the subsequent round. After four iterations, we ensure that each ambiguous instruction indexes three valid task grounding results and unseen regions, thereby completing the filtering pipeline.

B.4 Affordance Scoring Dimension Definition

The definitions of the affordance scoring dimensions are illustrated in Figure 8. The 19 dimensions include color complexity, glossiness, shape design, symmetry, surface smoothness, material, handle design, capacity, opening size, stability, transparency, material flexibility, volume, height-to-width ratio, durability, maintenance difficulty, safety, ease of use, and portability, collectively capturing the key appearance and functional traits of tools.

<i>Color Complexity</i> (0: None/Single color, 1-3: Simple, 4-6: Some variation, 7-9: Rich colors, 10: Extremely complex and natural colors)
<i>Glossiness</i> (0: No gloss, 1-3: Matte, 4-6: Slight shine, 7-9: High gloss, 10: Mirror-like gloss)
<i>Shape Design</i> (0: No shape, 1-3: Simple, 4-6: Moderately complex, 7-9: Unique/detailed, 10: Extremely artistic/complex)
<i>Symmetry</i> (0: Completely asymmetrical, 1-3: Unbalanced, 4-6: Mostly balanced, 7-9: Highly symmetrical, 10: Perfect symmetry)
<i>Surface Smoothness</i> (0: Very rough, 1-3: Noticeably rough, 4-6: Slight texture, 7-9: Smooth, 10: Highly polished)
<i>Material</i> (0: Unidentifiable, 1-3: Basic (wood/rubber), 4-6: Plastic, 7-9: High-quality (metal/ceramic), 10: Special material)
<i>Handle Design</i> (0: No handle, 1-3: Very basic, 4-6: Functional but not ergonomic, 7-9: Comfortable grip, 10: Extremely ergonomic)
<i>Capacity</i> (0: None, 1-3: Very small, 4-6: Moderate, 7-9: Large, 10: Very large)
<i>Opening Size</i> (0: No opening, 1-3: Very narrow, 4-6: Moderate, 7-9: Large, 10: Extra wide)
<i>Stability</i> (0-10: From extremely unstable to nearly impossible to tip over)
<i>Transparency</i> (0-10: From completely opaque to fully transparent)
<i>Material Flexibility</i> (0-10: From rigid and brittle to highly flexible and durable)
<i>Volume</i> (0-10: From tiny to very large in size)
<i>Height-to-Width Ratio</i> (0-10: From extremely flat to very tall and narrow)
<i>Durability</i> (0-10: From very fragile to nearly indestructible)
<i>Maintenance Difficulty</i> (0-10: From very hard to clean to extremely easy to maintain)
<i>Safety</i> (0-10: From highly dangerous to completely safe)
<i>Ease of Use</i> (0-10: From very difficult to extremely intuitive and convenient)
<i>Portability</i> (0-10: From not portable at all to ultra-portable and easy to carry)

Figure 8: Definition of the affordance scoring dimensions, encompassing both the appearance and functional traits of tools.

C Additional ablation studies

C.1 Ablation on core parts

In the paper, we have already presented ablation studies on the MSI and ADM streams of the AIDE framework. Here, we further report ablation results for the MM-CoT, ERS, and Exploration Policy, as summarized in Table 6. As shown in the table, without the involvement of the Exploration Policy, the task grounding results produced by MM-CoT and ERS fail to handle scenarios in which the required tools are not detectable and exploration is necessary. Consequently, compared to the setting with the Exploration Policy enabled, all success rate metrics of MM-CoT and ERS on both test sets decrease by at least 10%.

C.2 Ablation on affordance-based retrieval

Table 7 reports ablation results on retrieval methods and hyperparameter settings for upstream instruction retrieval in the ERS of the AIDE framework. Using the 432 ambiguous instructions in the Instruction-Tool Relationship Space as the retrieval corpus, retrieval accuracy and runtime are evaluated on all 100 instructions of the G-Dataset and the R-Dataset. For each test instruction, the instruction text is used as the input to the evaluated retrieval method under varying threshold values. As described in the paper, “Specifically, given the input instruction, the scheme performs an affordance-based depth-first search (DFS) over clusters in the relationship space until selecting an instruction whose affordance vector lies within a Euclidean distance c of the input.” The instruction identified through this process is treated as the validated retrieval result and is used for retrieval accuracy evaluation.

Compared with the affordance-based instruction retrieval method adopted in the paper, we conduct ablation studies to evaluate its performance against a text similarity-based instruction retrieval method. The latter uses the same set of instructions indexed in the Instruction-Tool Relationship Space as the retrieval corpus, but directly applies BGE-VL to compute textual similarity between the input instruction and the stored instructions, performing DFS based on these similarity scores (The DFS terminates when an instruction whose

textual similarity to the input instruction exceeds sim is retrieved.). For both methods, we further carry out extensive ablations on the DFS termination threshold. In addition, for each method, we also evaluate an exhaustive search baseline that compares the input instruction against all stored instructions without hyperparameter tuning.

As shown in Table 7, for the affordance-based instruction retrieval method, retrieval time decreases with the c , while accuracy peaks at 96.0% for $c = 10$. The exhaustive method yields slower retrieval than $c = 10$ and only 83.0% accuracy, 13.0% below the peak. The optimal performance at $c = 10$ reflects a balance between search depth and cluster discrimination: lower c truncates affordance-based deep matches, while higher c and exhaustive search weaken affordance-based cluster constraints, as well as overemphasize isolated neighbors, leading to misclassification of ambiguous inputs. Only at $c = 10$ does the method achieve both peak accuracy and near-minimal retrieval time compared with exhaustive search method and other c settings. For the textsim-based instruction retrieval method, retrieval time increases with the sim , while accuracy peaks at 87.0% for $sim = 0.7$, with the reason similar to that of the affordance-based method. However, because textsim-based instruction retrieval method is not fully grounded in affordance, this method exhibits a significant drop in retrieval accuracy compared to the affordance-based method, while also incurring substantially longer retrieval time, thereby confirming the empirical effectiveness of the affordance-based instruction retrieval design, and the benefit of the affordance scoring method brought to ambiguous instruction understanding.

D Details of Exploration Policy

Here we provide a more detailed explanation of the entry conditions for the Exploration Policy and the selection of exploration strategies. As introduced in the paper, if the maximum similarity between the top N candidate tools (detected by YOLO-World ranked by detection confidence) and tool images of retrieved candidate task planning results is below m , the Exploration Policy is triggered. Depending on whether the maximum similarity between the top $2N$ candidate tools

Method	G-Dataset						R-Dataset					
	TSR	OSR	FSR	WSR	ASR	FPS	TSR	OSR	FSR	WSR	ASR	FPS
MM-CoT	73.5	72.0	67.5	63.5	-	0.03	82.0	77.5	76.0	73.0	-	0.03
ERS	79.5	66.5	71.5	61.0	-	9.50	83.0	72.0	76.0	69.0	-	9.80
AIDE (w/o ADM)	90.5	89.0	84.5	80.5	68.0	0.03	96.0	91.5	90.0	87.0	70.0	0.03
AIDE (w/o MSI)	92.5	79.5	84.5	74.0	52.0	9.70	93.0	82.0	86.0	79.0	50.0	9.50
AIDE (Full)	94.5	88.0	89.0	83.0	64.0	9.70	95.0	92.0	91.0	88.0	65.0	9.50

Table 6: Ablation study on different components of AIDE. AIDE (w/o ADM) and AIDE (w/o MSI) represent AIDE variants that rely solely on the designed MSI and ADM, respectively, while AIDE (Full) represents the complete framework comprising both MSI and ADM.

Method	Threshold	Time (s)	Acc (%)
Affordance Retrieval	40	0.0001	20.0
	20	0.0020	72.0
	10	0.0046	96.0
	0	0.0065	83.0
	ES	0.0040	83.0
TextSim Retrieval	0.5	0.0524	35.0
	0.6	0.1511	70.0
	0.7	0.2395	87.0
	0.8	0.2973	84.0
	1	0.4134	80.0
	ES	0.2647	80.0

Table 7: Comparison of instruction retrieval runtime and accuracy under different hyper-parameter settings. “Affordance Retrieval” denotes the instruction retrieval method completely based on affordance. “TextSim Retrieval” denotes the instruction retrieval method based on text similarity matching. “ES” denotes an exhaustive search method that does not involve any threshold.

and all retrieved tool images is above or below 0.75, the Exploration Policy performs visible or invisible exploration and outputs the corresponding exploration region.

It is also important to emphasize that, regardless of whether the input to the Exploration Policy originates from MM-CoT or ERS, the entry conditions for exploration and the procedure for selecting exploration strategies remain exactly the same. Specifically, even when the input is provided by MM-CoT, retrieved candidate task planning results are first obtained through a process analogous to that used in ERS, and exploration is then conducted strictly following the procedure described above.

E Details of ADM

As stated in the paper, “The MSI stream is invoked once for key decision-making when the task is novel or ADM fails to identify any valid tool-related object in the updated scene (by applying a threshold based on the detection confidence produced and similarity matching).” In this section, we provide a more detailed description of the threshold design used by ADM to determine whether a valid tool-related object exists. Specifically, if both the detection confidence of a detected object (measured by YOLO-World) and the maximum similar-

ity between this object and all images in the existing tool retrieval library (measured by MobiliCLIP) are low, it is highly likely that the detected object is not valid. Accordingly, we define a criterion such that when the sum of (i) the detection confidence of the detected tool and (ii) the maximum similarity score between this tool and any tool image associated with the retrieved candidate task planning results is below 0.5, ADM is considered to have failed to identify any valid tool-related object in the updated scene, and the AIDE switches to the MSI stream. Otherwise, the ADM stream continues unchanged.

F Cost analysis

As described in the paper, generating task planning results as the content of the Instruction-Tool Relationship Space requires calling the GPT-5 API during the content generation stage. Specifically, the construction of the Task Planning Dataset, which serves as the content of the Instruction-Tool Relationship Space, involves additional filtering and regeneration steps to ensure the validity of the task planning results, resulting in a total cost of approximately \$260. Both the construction of the Instruction-Tool Relationship Space and the task planning process in the MSI stream incur an average cost of approximately \$0.04 per generated task planning result. In contrast, the ADM process, which accounts for the majority of frames in task planning and execution, does not involve any GPT-5 API calls and therefore incurs zero API cost. The manual screening effort mainly consists of removing instructions that are far from cluster centroids in the Task Planning Dataset (approximately 8.8% of all instructions) and verifying the validity of all remaining data points (see B.3). This manual process is assisted by GPT-5-based format validation. The Instruction-Tool Relationship Space occupies approximately 7.9 GB of disk storage.

G Real-World experiment video

As introduced in the paper, we evaluate AIDE on six novel tasks in unfamiliar environments to demonstrate its generalization capability. The provided folder contains a video showcasing the performance of a real robot on six randomly instantiated tasks: “I am thirsty”, “I want to clean the dust”, “I want to crack walnuts”, “I want something cold to drink”, “I want to close up delivery boxes tightly”, and “I want to support my waist while sitting”. As shown in Figure 9, the video

presents the execution process from wide-angle to close-up views, including third-person and first-person perspectives, fully demonstrating the performance of the AIDE method, such as closed-loop decision-making speed and accuracy, as well as the effectiveness of its guidance for robot interaction and execution. In particular, for the task “I want something cold to drink” and “I want to close up delivery boxes tightly”, interactive exploration is emphasized, while the grasping step is omitted due to its redundancy with the final grasping steps in other tasks. For statistical details of the experimental results, please refer to the paper.

H Detailed Error Analysis

1) Task planning and execution error: As introduced in the paper, AIDE may encounter planning-level and perception-level errors during task planning and execution. Planning-level errors arise from incorrect task understanding, potentially causing planning or execution failures. When these occur in ADM, the system checks for valid tool-related objects and switches to MSI if none are found. Failures in MSI are often due to occasional hallucinations from GPT-5, despite the MM-CoT design, and can be mitigated through human interaction for tool re-identification and further exploration. Perception-level errors occur when task understanding is correct but visual degradation from robot motion causes small offsets in area-tool positioning. These manifest as sporadic single-frame deviations amid predominantly correct execution frames, and do not impact overall task completion.

2) Affordance label error: All instructions in the Instruction-Tool Relationship Space are first generated by GPT-5 and then scored based on the physical and functional traits of the tools required to accomplish each instruction. Through extensive experiments and comparative analyses, we identify 19 dimensions among the candidate scoring dimensions that most effectively capture tool traits and best discriminate between different instructions and tools; these 19 dimensions are therefore selected as the final affordance-based scoring dimensions. As discussed in the paper, the many-to-many relationships between instructions and tools ensure that occasional errors in individual affordance labels within the relationship space have a negligible impact on task-planning-related decision-making.

3) Hallucination error: Although GPT-5, the segmentation model SAM2, and the object detection model YOLO-World used in the MM-CoT module of AIDE all exhibit strong capabilities, our experiments reveal that GPT-5 and the grounding models respectively suffer from hallucination and performance instability. As a result, directly applying them to task grounding in AIDE is inappropriate. We therefore adopt dedicated mitigation strategies for each.

To address hallucination in GPT-5, we leverage prior findings that Chain-of-Thought (CoT) reasoning can alleviate hallucinations. Through extensive experimentation and by building upon existing approaches, we design precise multimodal CoT strategies and prompt formulations, which substantially reduce hallucinations induced by GPT-5. In addition, as described in the paper, one of the core design goals of the ADM stream in AIDE is to mitigate GPT-5-induced hallu-

cinations during task planning by constructing a comprehensive Instruction-Tool Relationship Space. The task planning results generated with GPT-5 involvement within this relationship space are further filtered using a principled pipeline, as detailed in B.3, to remove erroneous outputs. Moreover, as described in 1), when errors occur in task planning results produced by the GPT-5-based MSI stream, AIDE incorporates human-in-the-loop interactions, including tool re-localization and re-exploration, as additional mechanisms to mitigate GPT-5 hallucinations.

Regarding the instability of the segmentation model SAM2 and the object detection model YOLO-World, we observe that the default configuration of SAM2 fails to precisely segment the required tools or critical regions, while adjusting the segmentation granularity leads to inconsistent performance across scenes of different scales. To address this issue, we draw inspiration from the SoM approach and configure SAM2 to operate at the finest segmentation granularity, ensuring that collections of segmented regions can jointly form complete tools or key areas of interest. These labeled regions are then provided to GPT-5. And GPT-5 determines which subsets of segments correspond to the target tools or key regions. The regions selected according to GPT-5’s output are used as the final segmentation results. Experimental results demonstrate that this cross-verification between GPT-5 and the segmentation model significantly improves SAM2’s segmentation performance in our experimental setting. For YOLO-World, although it is a powerful open-vocabulary object detection model, we find that it performs poorly in identifying tool-specific key regions (e.g., handles and bodies) and frequently produces overlapping detection boxes. To mitigate these issues, we first carefully design the detection text prompts and apply Non Maximum Suppression (NMS) to ensure that the top five candidates ranked by detection confidence include the target object. We then employ the matching and similarity comparison strategies introduced in the ERS, leveraging the constructed comprehensive retrieval list to identify the true target among these candidates.



Figure 9: The tasks of the six real-world experiments include processes such as positioning, tool understanding, and interactive exploration, and are executed at 10Hz.

I Model information

All models used in the paper are summarized in Table 8.

Model Name	Model ID	Size
GPT-5	gpt-5	Unknown
Molmo-7B-D	allenai/Molmo-7B-D-0924	7B
Qwen 3 VL-30B Instruct	Qwen/Qwen3-VL-30B-A3B-Instruct	30B
Magma-8B	microsoft/Magma-8B	8B
RoboPoint	wentao-yuan/robopoint-v1-vicuna-v1.5-13b	13B
SAM2	facebook/sam2.1-hiera-large	856M
MobileCLIP	apple/MobileCLIP-B-LT	599M
YOLO-World	yolov8x-worldv2	139M
YOLO-World	yolov8l-worldv2	89M
BGE-VL	BAAI/BGE-VL-large	428M

Table 8: Models used in this paper. In the actual experiments, yolov8x-worldv2 is used for detecting tools and exploration regions, while yolov8l-worldv2 is employed for detecting key regions of tools.

J Extended Applications of AIDE

To further validate the effectiveness of the proposed AIDE method, we deploy AIDE on a humanoid robot in both simulated and real-world environments to perform embodied planning tasks such as box carrying, including task planning and execution. Representative processes and results are illustrated in Figure 10. These experiments further demonstrate the effectiveness of AIDE as well as its potential for real-world deployment.



Figure 10: Deployment of the AIDE method in the humanoid robot simulation environment (left) and real-world environment (right).

K Code structure

Alg. 1 outlines the inference process of the Efficient Retrieval Scheme (ERS) given a single instruction and scene image. For convenience, Alg. 1 directly illustrates the final exploration results, where the outputs of ERS are first filtered by a thresholding criterion and then passed to the Exploration Policy. After loading the required multimodal retrieval and object detection models, the ERS retrieves a set of candidate task planning results most similar to the input instruction based on affordance scores and predefined thresholds c and d . It then employs the YOLO-World and MobileCLIP to locate tool region. If the maximum similarity between the top N candidate tools and tool images of retrieved candidate task planning results is below m , the Exploration Policy is triggered. Depending on whether the maximum similarity T_{new} between the top $2N$ candidate tools and all retrieved tool images is above or below 0.75, the system performs visi-

ble or invisible exploration and outputs the corresponding exploration region. Otherwise, exploration is skipped, and the system proceeds to identify and output the tool’s operational and functional region coordinates.

Implementation details are provided in the code appendix, and all source code required for conducting and analyzing the simulation and real-world experiments will be made publicly available upon publication of the paper with a license that allows free usage for research purposes.

Algorithm 1 Efficient Retrieval Scheme (ERS)

Input: input instruction I_{ins} , input scene image I_{img} , encoded data D_{enc} , score matrix S
Parameter: $c = 10, d = 15, m = 0.85, N = 5, N' = 40, PX = 250$
Output: target region B_{out}

- 1: $(M_{\text{CLIP}}, M_{\text{YOLO}}) \leftarrow \text{LoadModel}()$
- 2: $I \leftarrow (I_{\text{img}}, I_{\text{ins}})$
- 3: $\text{root} \leftarrow \text{LibraryConstruction}(D_{\text{enc}})$
- 4: $\text{IdxSingle} \leftarrow \text{SimilarityCalculation}(\text{root}, I, c)$
- 5: $\text{Idx} \leftarrow \text{ScoreBasedSelection}(\text{IdxSingle}, S, d)$
- 6: $(S_{\text{max}}, T_{\text{new}}, B_{\text{tool}}) \leftarrow \text{SearchWholeProcess1}(\text{Idx}, I, D_{\text{enc}}, M_{\text{YOLO}}, M_{\text{CLIP}}, N)$
- 7: **if** $S_{\text{max}} < m$ **then**
- 8: **if** $T_{\text{new}} > 0.75$ **then**
- 9: $B_{\text{vis}} \leftarrow \text{VisibleExploration}(I_{\text{img}}, M_{\text{YOLO}}, N, N', PX)$
- 10: $B_{\text{out}} \leftarrow B_{\text{vis}}$
- 11: **else**
- 12: $B_{\text{inv}} \leftarrow \text{InvisibleExploration}(I, M_{\text{YOLO}}, M_{\text{CLIP}}, D_{\text{enc}}, N)$
- 13: $B_{\text{out}} \leftarrow B_{\text{inv}}$
- 14: **end if**
- 15: **else**
- 16: $(B_{\text{op}}, B_{\text{fn}}) \leftarrow \text{SearchWholeProcess2}(\text{Idx}, I, D_{\text{enc}}, M_{\text{YOLO}}, M_{\text{CLIP}}, N)$
- 17: $B_{\text{out}} \leftarrow (B_{\text{tool}}, B_{\text{op}}, B_{\text{fn}})$
- 18: **end if**
- 19: **return** B_{out}
